International Journal of Pure and Applied Mathematics
Volume 23 No. 3 2005, 365-378

AN ACCURATE HIGH-ORDER METHOD TO SOLVE THE HELMHOLTZ BOUNDARY VALUE PROBLEM FOR THE 3D LAPLACE EQUATION

Shashikant Manikonda[1], Martin Berz[2 §]
[1,2]Department of Physics and Astronomy
Michigan State University
East Lansing, MI 48824, USA
[1]e-mails: manikond@msu.edu
[2]e-mails: berz@msu.edu

Abstract: The 3D Laplace equation is one of the important PDEs of physics and describes the phenomonology of electrostatics and magnetostatics. Frequently very precise solution of this PDE is required; but with conventional finite element or finite difference codes this is difficult to achieve because of the need for an exceedingly fine mesh which leads to often prohibitive CPU time.

We present an alternate approach based on high-order quadrature and a high-order finite element method. Both of the ingredients become possible via the use of high-order differential algebraic methods. Various examples of the method and the precision that can be achieved will be given. For example, using only about 100 finite elements of order 7, accuracies in the range of 10^{-6} can be obtained in the 3D case.

AMS Subject Classification: 33F99, 35J05, 65N99
Key Words: Laplace equation, Helmholtz Theorem, differential algebra

1. Introduction

In this paper, we study some methods for finding highly accurate numerical approximations of the solution of the Laplace equation

Accepted: June 27, 2005

§Correspondence author

$$\Delta\psi\left(\overrightarrow{r}\right) = 0$$

in the volume $\Omega \subset \mathbb{R}^3$under specification of $\vec{\nabla}\psi\left(\overrightarrow{r}\right)$ on the surface $\partial\Omega$. This equation is of particular interest in science and engineering because it describes static problems in electromagnetism, heat conduction, and a variety of other important problems. The existence and uniqueness of solutions for the 3D case can easily be shown through the application of Green's formulae; in particular, it is well-known that specification of the derivative of ψ is sufficient for uniqueness of the solution.

However, in many practical cases the full gradient of ψ is available, and the methods we develop will take into account this additional information. For example, in the electric or magnetic case measuring the fields $\vec{E}$ or $\vec{B}$ on the surface $\partial\Omega$ entails the knowledge of the full $\vec{\nabla}\psi$ and not only the component that happens to be normal to the surface. Furthermore, if $\partial\Omega$ happens to follow metal, it is known a priori from physical reasons that the non-normal components of $\vec{\nabla}\psi$ vanish.

It is well known that analytic closed form solutions for the 3D case can be found for problems with certain regular geometries where a separation of variables can be performed. However, in most practical 3D cases, numerical methods are the only way to proceed. Usually the finite difference or finite element approach are used to find the numerical solution as data set in the region of interest. But because of their usually relatively low approximation order, for the problem of precise solution of PDEs, the methods have limited success because of the prohibitively large number of cells required.

In the following, we develop a method that determines local finite elements of in principle unlimited order, and show results of computations up to order 9 which allow to achieve unusually high accuracy with unusually few cells. In Section 2 we discuss the benefits of using boundary data and present the analytic closed form solution for the 2D case that can be easily found by application of Cauchy's integral formula. We then use a 2D example to highlight the advantages of the methods that use the boundary data to compute the solution.

In Section 3 we present the theory and the implementation of the new scheme to find the solution of the 3D Laplace equation with the gradient boundary conditions. This scheme is based on the Helmholtz Theorem and the differential algebraic tools [1] of the code *COSY Infinity* [3, 2]. We conclude with an application of this new scheme to a 3D magnetostatic problem.

2. Methods Using Boundary Data

The methods developed in the subsequent sections are based on representing the solution in terms of surface integrals. These methods based on boundary data have the following basic desirable properties:

1. The approximate solution obtained for the inside is infinitely often differentiable because the so-called "kernel" in the integral is. This allows the use of Taylor expansion techniques for the representation of the solution.

2. If the boundary data have errors, as long as they represent a harmonic function, the resulting errors on the inside will not exceed those of the surface errors because of the well-known fact that harmonic functions assume their maximum on the boundary. This is particularly important for the analysis of the consequences of systematic errors.

3. If the boundary data have randomly distributed errors, the process of integration over the surface will tend to average those out. Thus the resulting solution on the inside will often be significantly more accurate than the data on the surface.

2.1. The Two Dimensional Case

As an introduction to the general approach, we begin with the discussion of the 2D case. The theory of this case can be fully developed within the framework of elementary complex analysis, which makes the entire method rather transparent. Cauchy's integral formula states that if the complex function f is analytic in a region containing the path C, and if α is a point in the interior of C, then

$$f(a) = \frac{1}{2\pi i} \oint_C \frac{f(z)}{z-\alpha} dz\,, \tag{1}$$

where the integral denotes the path integral over C. Cauchy's formula is an integral representation of f which permits us to compute f anywhere in the interior of C based on the value of f on C. Let now $\vec{f} = (f_x, f_y) : \mathbb{R}^2 \to \mathbb{R}^2$ with $f_x = \mathrm{Re}(f)$ and $f_y = -\mathrm{Im}(f)$. Because of the Cauchy-Riemann conditions, we have that $\partial f_x/\partial y = \partial f_y/\partial x$, and thus $\vec{f}$ admits a potential F, which in turn satisfies $\partial^2 F/\partial x^2 + \partial^2 F/\partial y^2 = 0$. Furthermore, F can be computed from $\vec{f}$ by mere integration (in R^2) over an arbitrary path. Thus F is a solution to the $2D$ Laplace equation the gradient of which is specified

on C, and it can be computed in terms of an integral over the surface followed by a simple path integral.

For the purpose of illuminating the method, we choose an example where the path C is a circle enclosing the region of interest. We divide the perimeter of the circle into equal 500 subsections of half length $l = 4\pi/500/2 \approx 0.0125$ each. For the point $\alpha = 1 + i$ inside the circle of radius 2, we look at the Taylor expansion of the integral kernel $1/(z - \alpha)$ with respect to the arc length variable at the point $s_0 = \sqrt{3}+i$ on the circle. The expansion is carried out using high-order automatic differentiation in the variable $(s-s_o)\cdot l$, where s_0 is the center of the subsection. The resulting real and imaginary parts of the coefficients of this expansion are:

I	COEFFICIENTS		ORDER
1	0.000000000000000	-.2174096954013957	0
2	0.1292820323027551E-01	0.7464101615137748E-02	1
3	-.5125145207369106E-03	0.5125145207369108E-03	2
4	-.9429469459320545E-05	-.2576178965128279E-04	3
5	0.1358429640429984E-05	0.4104759770491565E-06	4
6	-.3573701117784867E-07	0.6828212126069532E-07	5
7	-.1625148053818077E-08	-.1387364193455211E-08	6
8	0.1262955182214571E-09	0.6248216385868244E-10	7
9	-.2137193331532445E-11	0.1186779665333633E-10	8
10	-.2256154520790502E-12	0.2963052833686976E-12	9
11	0.9935878898026400E-14	0.3377579654709185E-13	10
12	-.1417190659393024E-15	0.3712825785891593E-14	11

It can be seen that in this expansion, the contributions of higher order terms decrease rapidly. Thus it is possible to obtain an approximation of the Cauchy path integral equation (1) by merely integrating the Taylor polynomial on each of the separate parts of the integration path. The overall accuracy of this approach will be approximately that of the accuracy of each expansion; so carrying the expansion to order 10, we may expect an accuracy around 10^{-14}.

3. The Three Dimensional Case

References [8, 6] provide extensions to the Cauchy's Integral Formula to higher dimensions. The scheme we use for the 3D case is based on the Helmholtz vector decomposition theorem; see for example [7, 11, 12, 9, 10].

We begin by representing the solution of the PDE via Helmholtz' Theorem, which states that any vector field $\overrightarrow{B}$ which vanishes at infinity can be

written as

$$\overrightarrow{B}(\vec{x}) = \vec{\nabla} \times \vec{A}_t(\vec{x}) + \vec{\nabla}\phi_n(\vec{x}) \,, \tag{2}$$

where

$$\phi_n(\vec{x}) = \frac{1}{4\pi}\int_{\partial\Omega} \frac{\vec{n}(\vec{x}_s)\cdot\overrightarrow{B}(\vec{x}_s)}{|\vec{x}-\vec{x}_s|}ds - \frac{1}{4\pi}\int_{\Omega} \frac{\vec{\nabla}\cdot\overrightarrow{B}(\vec{x}_v)}{|\vec{x}-\vec{x}_v|}dV \text{ and}$$

$$\vec{A}_t(\vec{x}) = -\frac{1}{4\pi}\int_{\partial\Omega} \frac{\vec{n}(\vec{x}_s)\times\overrightarrow{B}(\vec{x}_s)}{|\vec{x}-\vec{x}_s|}ds + \frac{1}{4\pi}\int_{\Omega} \frac{\vec{\nabla}\times\overrightarrow{B}(\vec{x}_v)}{|\vec{x}-\vec{x}_v|}dV \,.$$

Here $\partial\Omega$ is the surface which bounds the volume Ω. $\vec{x}_s$ denotes a point on the surface $\partial\Omega$, and $\vec{x}_v$ denotes a point within Ω. $\vec{n}$ is the unit vector perpendicular to $\partial\Omega$ that points away from Ω. $\vec{\nabla}$ denotes the gradient with respect to $\vec{x}_v$.

If the curl and divergence of $\vec{B}$ vanish, which is the case for the field described by the potential obtained from Laplace's equation, then the volume integral terms vanish, and $\phi_n(\vec{x})$ and $\vec{A}_t(\vec{x})$ are completely determined from the normal and the tangential component of $\vec{B}$ on the surface $\partial\Omega$ as

$$\phi_n(\vec{x}) = \frac{1}{4\pi}\int_{\partial\Omega} \frac{\vec{n}(\vec{x}_s)\cdot\overrightarrow{B}(\vec{x}_s)}{|\vec{x}-\vec{x}_s|}ds \,, \tag{3}$$

$$\vec{A}_t(\vec{x}) = -\frac{1}{4\pi}\int_{\partial\Omega} \frac{\vec{n}(\vec{x}_s)\times\overrightarrow{B}(\vec{x}_s)}{|\vec{x}-\vec{x}_s|}ds. \tag{4}$$

For any point within the volume Ω, the scalar and vector potentials depend only on the field on the surface $\partial\Omega$. Furthermore, the interior fields will be analytic even if the field on the surface data fails to be differentiable. To conclude we mention in passing that there are also various higher dimensional extensions to the Helmholtz Theorem [14, 13] which may be useful to also solve certain four dimensional boundary value problems.

3.1. Surface Integration and Finite Elements via Differential Algebraic Techniques

Since the expressions in equations (3) and (4) are analytic if $\vec{x}$ is not on the surface, they can be approximated by a Taylor expansion, which for small enough domains is expected to represent the function well. The idea is now to expand them to higher orders in BOTH the two surface variables $\vec{x}_s$ and the three volume variables $\vec{x}$. The dependence on the surface variables will be integrated over surface sub-cells, which results in a highly accurate integration formula with an error order equal to that of the expansion.

The volume Ω is subdivided into volume elements. Using the prescription for the surface field, the Taylor expansion of the field is computed at the center of each volume element. The dependence on the volume variables will thus be retained in polynomial form, which leads to a high order finite element method. By using sufficiently high order, high accuracy can be achieved with a small number of surface elements, and more importantly, a small number of volume elements. The final solution inside the overall volume is thus given by local expansions of the field in each of the volume elements.

To find the local expansions for each volume element, we first split the domain of integration $\partial\Omega$ into smaller elements Γ_i. From the surface field formula we extract approximate Taylor expansion in the surface variables $\vec{x}_s$ about the center of the surface element. Then the integral kernel $1/\left|\vec{r}-\vec{r}_s\right|$ and the field $\vec{B}$ on the surface are Taylor expanded in the surface variables $\vec{r}_s$ about the center of each surface element. We also Taylor expand the kernel in the volume variables $\vec{r}$ about the center of the volume element. All these operations are performed automatically using the differential algebraic tools in the code *COSY*, see [3, 2, 1]. The final step is to integrate and sum the resulting Taylor expansions for all surface elements. Depending on the accuracy of the computation needed we choose step sizes, order of expansion in the three volume variables and order of expansion in the two surface variables s_1 and s_2.

We obtain the scalar potential $\phi_n\left(\vec{x}\right)$ by choosing the integrand $g(x,y) = \vec{n}_s \cdot \vec{B}\left(\vec{x}_s\right)/\left|\vec{r}-\vec{r}_s\right|$, and the vector potential $\vec{A}_t\left(\vec{x}\right)$ by choosing $g(x,y) = \vec{n}_s \times \vec{B}\left(\vec{x}_s\right)/\left|\vec{r}-\vec{r}_s\right|$. The field $\overrightarrow{B}\left(\vec{x}\right)$ can be computed using equation (2). All the mathematical operation to perform the expansion, surface integration, curl and divergence were implemented using the high-order multivariate differential algebraic tools [1] available in the code *COSY Infinity*, see [3, 2], and they directly allow to obtain the finite elements to arbitrary order.

4. An Analytical Example: The Bar Magnet

As a reference problem we consider the magnetic field of an arrangement of two rectangular iron bars with inner surfaces ($y = \pm y_0$) parallel to the mid-plane ($y = 0$) . The interior of these uniformly magnetized bars, which are assumed to be infinitely extended in the $\pm y$-directions, is defined by: $x_1 \le x \le x_2$, $|y| \le y_0$, and $z_1 \le z \le z_2$. From this bar magnet one can obtain an analytic solution for the magnetic field $\vec{B}\left(x,y,z\right)$ – see for example

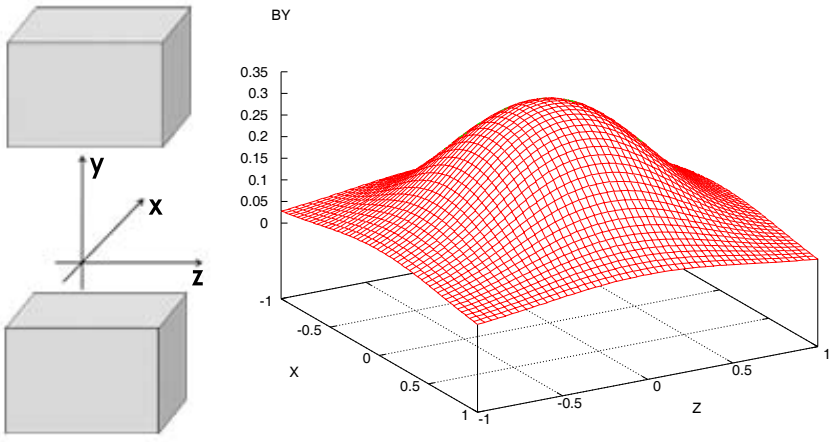

(a) (b)

Figure 1: (a) Geometric layout of the bar magnet, consisting of two bars of magnetized material. (b) Magnetic field B_y on the center plane of the bar magnet. $B_0 = 1T$ and the interior of this magnet is defined by $-0.5 \leq x \leq 0.5$, $|y| \leq 0.5$, and $-0.5 \leq z \leq 0.5$

[4, 5] - and the result is given by

$$
\begin{aligned}
B_y(x,y,z) &= \frac{B_0}{4\pi}\sum_{i,j}(-1)^{i+j}\left[\arctan\left(\frac{X_i\cdot Z_j}{Y_+\cdot R_{ij}^+}\right)+\arctan\left(\frac{X_i\cdot Z_j}{Y_-\cdot R_{ij}^-}\right)\right], \\
B_x(x,y,z) &= \frac{B_0}{4\pi}\sum_{i,j}(-1)^{i+j}\left[\ln\left(\frac{Z_j+R_{ij}^-}{Z_j+R_{ij}^+}\right)\right], \\
B_z(x,y,z) &= \frac{B_0}{4\pi}\sum_{i,j}(-1)^{i+j}\left[\ln\left(\frac{X_j+R_{ij}^-}{X_j+R_{ij}^+}\right)\right], \qquad (5)
\end{aligned}
$$

where $X_i = x - x_i$, $Y_\pm = y_0 \pm y$, $Z_i = z - z_i$, and $R_{ij}^\pm = \left(X_i^2 + Y_j^2 + Z_\pm^2\right)^{\frac{1}{2}}$. The geometric layout and mid plane field of such a magnet is shown in Figure 1.

We note that because of the symmetry of the fields in equation (5), only even order terms exist in the Taylor expansion of this field about the origin.

4.1. Results and Analysis

As a first step, we study the performance of the surface integration method. To this end, we consider a cube of edge length 0.8, whose center coincides with the center of the interior of the uniformly magnetized bars. The six surfaces of the cube are each subdivided into a 44×44 mesh. On each of the mesh cells, the contribution from the Helmholtz integral is expanded using differential algebraic tools [1], and the resulting polynomial is integrated. The Figure 2 shows the accuracy of the predicted field, compared with the exact solution, as a function of the order of expansion within the surface mesh cells. Results are shown for the points $(0, 0, 0)$, $(0.1, 0.1, 0.1)$, $(0.2, 0.2, 0.2)$ and $(0.3, 0.3, 0.3)$. It can be seen that at order six, an accuracy of approximately 10^{-12} is reached, which is very high compared to conventional numerical field solvers.

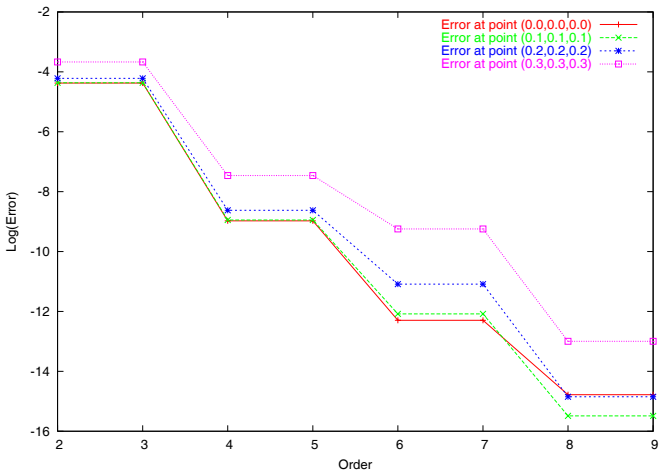

Figure 2: Error for the field calculated for the bar magnet example for individual points $(0, 0, 0)$, $(0.1, 0.1, 0.1)$, $(0.2, 0.2, 0.2)$ and $(0.3, 0.3, 0.3)$

We note that a change from an even order to the next higher order does not produce significant change in the error, which is due to the specific symmetry of the magnetic field and the resulting fact that even orders dominate in the Taylor expansion.

For the next example, we split the volume inside the bar magnet into $4 \times 4 \times 4$ finite elements of width ± 0.1. Within each of the elements, a Taylor

expansion in the three volume variables is carried out, resulting in a polynomial representation of the field within the finite element cell. The polynomial representation is used to evaluate the field at 1000 randomly chosen points within the cell, and comparing the result with the analytical answer. Figure 3 shows the resulting RMS error for finite elements centered around $(0, 0, 0)$, $(0.1, 0.1, 0.1)$, $(0.2, 0.2, 0.2)$ and $(0.3, 0.3, 0.3)$. The plot for the finite element centered at $(0.3, 0.3, 0.3)$ shows the behavior of the RMS error as we approach the boundary. It can be seen that the method remains stable as we approach the boundary. For the finite elements well within the volume of interest, it can be seen that at order 7, an accuracy of approximately 10^{-6} is reached.

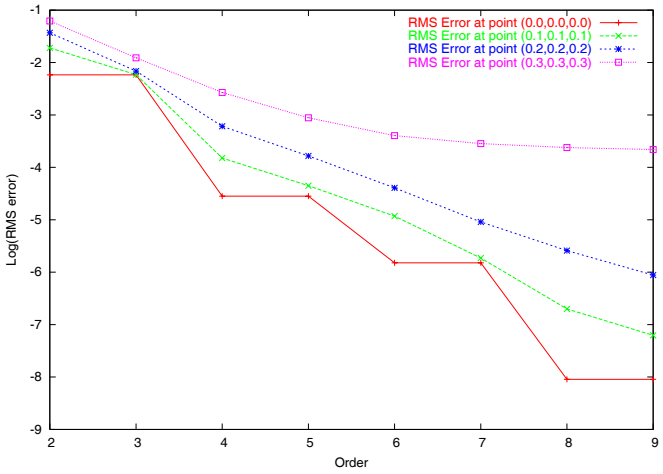

Figure 3: Average error for the field calculated for the bar magnet example for finite elements of total width 0.2 around points $(0, 0, 0)$, $(0.1, 0.1, 0.1)$, $(0.2, 0.2, 0.2)$ and $(0.3, 0.3, 0.3)$

We see that the method of simultaneous surface and volume expansion, all of which can be carried out fully automatically using differential algebraic tools [1] implemented in the code *COSY*, see [3, 2], leads to accuracies that are significantly higher than those of conventional finite element tools, even when unusually large finite elements are used.

For the purpose of illustration, we now show some of the resulting Taylor expansions. We begin with the resulting field equation (3) over one surface element centered at $(-0.39, -0.39, 0.4)$ and compute the field contributions at the point $(0.1, 0.1, 0.1)$. In the representation of the Taylor expansion

below, the entries in the first column provide the number assigned to each of the coefficients in the Taylor expansion to easily identify them. The entries in the second column provide the numerical value of the coefficients. The entries in the fourth, fifth and the sixth columns provide the expansion orders with respect to the volume variables (x, y, z). And the entries in the seventh and eighth column provide the expansion orders with respect to the surface variables (x_s, y_s). It can be seen that in this expansion, the contributions of higher order terms depending on the surface variables decrease rapidly, illustrating the rapid convergence of the method.

```
Sample eighth order Taylor expansion in two surface variables
     I  COEFFICIENT            ORDER EXPONENTS
     1  0.1430015055365947E-01   0   0 0  0 0  0
     2  0.6922600731781813E-03   1   0 0  0 1  0
     3  -.9437452710153340E-03   1   0 0  0 0  1
     4  -.1561210105220474E-04   2   0 0  0 2  0
     5  -.4471499751575185E-04   2   0 0  0 1  1

     ⋮

    20  -.3232493054085583E-07   5   0 0  0 1  4
    21  0.6156849473575023E-07   5   0 0  0 0  5
    22  0.8960505971632865E-10   6   0 0  0 6  0
    23  0.1890553337467643E-08   6   0 0  0 5  1
    24  -.9792219471281489E-09   6   0 0  0 4  2

    ⋮

    41  -.2417698920592542E-10   8   0 0  0 4  4
    42  0.7717865536738434E-10   8   0 0  0 3  5
    43  -.2649803372019223E-11   8   0 0  0 2  6
    44  -.2561415687161454E-10   8   0 0  0 1  7
    45  0.8506329051477273E-10   8   0 0  0 0  8
    -----------------------------------------
```

We now present the Taylor expansion of the field equation (3) over one surface element, and simultaneously over one volume element inside the volume of interest. The center of the surface element is at $(-0.39, -0.39, 0.4)$ and the center of the volume element is at $(0.1, 0.1, 0.1)$. In this case the coefficients of the Taylor expansion depend on both the surface and the volume variables. Once again we notice that the contributions of higher order terms decrease rapidly with an increase in order.

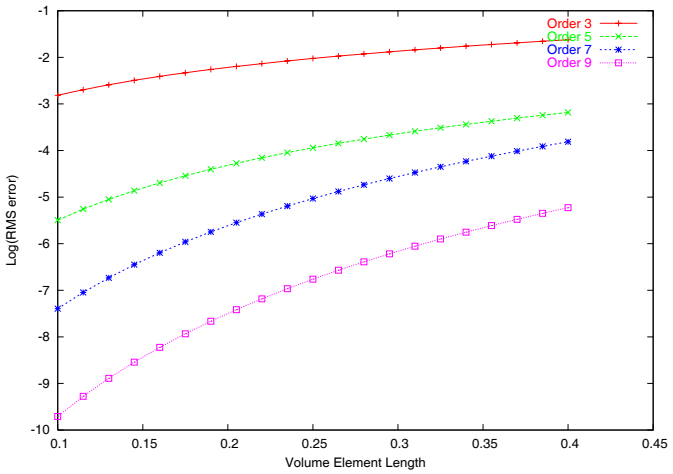

Figure 4: Average error VS volume element length

Sample eighth order Taylor expansion in two surface variable and three volume variables

I	COEFFICIENT	ORDER	EXPONENTS
1	0.1430015053365947E-01	0	0 0 0 0 0 0
2	-.9590481459719684E-02	1	1 0 0 0 0 0
3	-.9590481459719684E-02	1	0 1 0 0 0 0
4	-.9768082968233012E-02	1	0 0 1 0 0 0
5	0.6922600731781812E-03	1	0 0 0 1 0 0
⋮			
422	-.1498862045486747E-06	6	0 2 0 2 2
423	-.7743571762444490E-07	6	1 0 1 2 2
424	-.4431814352690413E-06	6	0 1 1 2 2
425	-.5355653167206839E-08	6	0 0 2 2 2
426	-.1876734453768074E-06	6	2 0 0 1 3
⋮			
1283	-.2417698920592547E-10	8	0 0 0 4 4
1284	0.7717865536738462E-10	8	0 0 0 3 5
1285	-.2649803372019148E-11	8	0 0 0 2 6
1286	-.2561415687161455E-10	8	0 0 0 1 7
1287	0.8506329051477271E-10	8	0 0 0 0 8

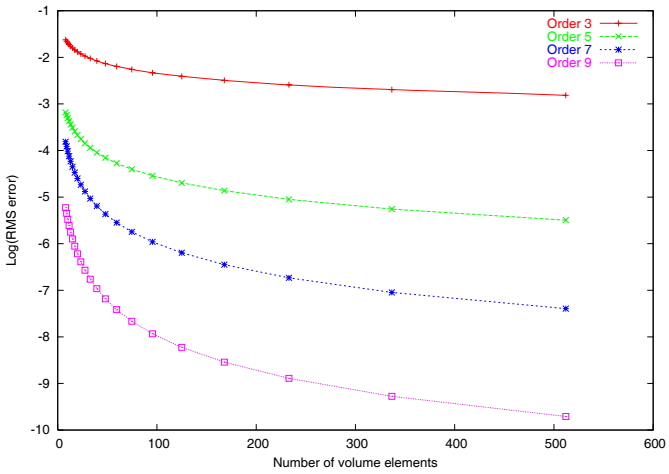

Figure 5: Average error VS number of volume elements

We now equivalently study the error dependency on the size (length) of the volume element or the number of volume elements chosen for the computation.

For the order of computation $3, 5, 7$ and 9, Figure 4 and Figure 5 provide the dependence of the average error on the length of the volume element and the total number of volume elements. As an example, for cell lengths of 0.1, which leads to a total number of only 550 finite elements, an accuracy of 10^{-10} can be reached with a ninth order method. Similarly, for a seventh order method with a cell length of 0.2, corresponding to 64 boxes, accuracies of about 10^{-6} can be reached.

References

[1] M. Berz, *Modern Map Methods in Particle Beam Physics*, Academic Press, San Diego (1999); Also available at http://bt.pa.msu.edu/pub

[2] M. Berz, J. Hoefkens, K. Makino, *COSY Infinity, Version 8.1 – Programming Manual*, Technical Report MSUHEP-20703, Department of Physics and Astronomy, Michigan State University, East Lansing, MI 48824 (2002); see also http://cosy.pa.msu.edu.

[3] M. Berz, K. Makino, *COSY Infinity, Version 8.1 – User's Guide and Reference Manual*, Technical Report MSUHEP-20704, Department of

Physics and Astronomy, Michigan State University, East Lansing, MI 48824 (2002); see also http://cosy.pa.msu.edu

[4] R. Degenhardt, M. Berz, High accuracy description of the fringe fields of particle spectrographs, In: *Proceedings 1993 Particle Accelerator Conference*, Washington, DC (1993).

[5] R. Degenhardt, M. Berz, High accuracy description of the fringe field in particle spectrographs, *Nuclear Instruments and Methods*, **A427** (1999), 151-156.

[6] D. G. Fulton, G. Y. Rainich, Generalizations to higher dimensions of the cauchy integral formula, *American Journal of Mathematics*, **54**, No. 2 (1932), 235-241.

[7] H.V. Helmholtz, Über Integrale der hydromechanischen Gleichung, welche den Wirbelbewegungen entsprechen, *J. Reine Angew. Math.*, **55**, No. 25 (1858).

[8] K.S Kunz, Application of an algebraic technique to the solution of laplace's equation in three dimensions, *SIAM Journal on Applied Mathematics*, **21**, No. 3 (1971), 25-441.

[9] M. Venturini, D. Abell, A. Dragt, Map computation from magnetic field data and application to the lhc high-gradient quadrupoles, *eConf.*, **C980914** (1998), 184-188.

[10] M. Venturini, A.J. Dragt, Accurate computation of transfer maps from magnetic field data, *Nuclear Instruments and Methods*, **A427** (1999), 387-392.

[11] P.L. Walstrom, Soft-edged magnet models for higher-order beam-optics map codes, *Nuclear Instruments and Methods*, **A519**, No. 1-2 (2004), 216-221.

[12] P. Walstrom, A. Dragt, T. Stasevich, Computation of charged-particle transfer maps for general fields and geometries using electromagnetic boundary-value data, In: *IEEE Particle Accelerator Conference 2001* (2001).

[13] Dale A. Woodside, Uniqueness theorems for classical four-vector fields in euclidean and Minkowski spaces, *Journal of Mathematical Physics*, **40**, No. 10 (1999), 4911-4943.

[14] Dale A. Woodside, Classical four-vector fields in the relativistic longitudinal gauge, *Journal of Mathematical Physics*, **41**, No. 7 (2000), 4622-4653.